NASA Technical Paper 1488

# Predicting Dynamic Performance Limits for Servosystems With Saturating Nonlinearities

John A. Webb, Jr., and Richard A. Blech

NASA

NASA Technical Paper 1488

# Predicting Dynamic Performance Limits for Servosystems With Saturating Nonlinearities

John A. Webb, Jr., and Richard A. Blech
*Lewis Research Center*
*Cleveland, Ohio*

# SUMMARY

When developing very high-response servosystems, the system's linear dynamics can be extended by compensation and feedback techniques. This leaves nonlinearities and power limits as the only practical limitations of the obtainable dynamic response. This report demonstrates a technique for predicting the dynamic performance limits of a system with saturations.

Generalized treatment for a system with a single saturating nonlinearity results in low- and high-frequency asymptotes for upper response bounds. The bounds are verified by comparing analytical results with frequency-response plots obtained from an analog computer model of the system. Once the amplitude dynamics are predicted with the limit lines, an iterative technique is employed to determine the system phase response.

The limit-line technique is then used in conjunction with previously derived velocity and acceleration limits for electrohydraulic servosystems to predict the maximum dynamic performance obtainable for an electrohydraulic servosystem containing a single-stage servovalve. The servovalve used in this system was a single-stage electrohydraulic design that provides linear dynamic capabilities beyond the range of conventional two-stage electrohydraulic servovalves. By deriving relationships that define the upper bound on system performance, those system parameters that affect these bounds can be identified. The resulting design criteria can be used to optimize the system design.

The predicted maximum performance for the servosystem is compared with experimentally obtained response data. The results demonstrate that the limit-line predictions agree quite well with the data. The optimized system exhibited an amplitude response that was flat to within ±3 decibels of the commanded amplitude for frequencies to 530 hertz for a peak-to-peak displacement of 0.127 centimeter and a load mass of 1.1 kilograms.

# INTRODUCTION

Electrohydraulic, servoactuated air valves have been used extensively as research control and perturbation devices on turbojet engines and supersonic inlets (refs. 1 to 3). As perturbation devices, they provide a means for creating pressure or flow perturbations in the normal flow processes of engine components. Dynamic analysis of the resulting signals provides transfer-function models that can be used to describe the system (refs. 4 and 5). When these valves are placed in control loops, they can be used for

stabilizing unstable flow phenomena or for studying control techniques (ref. 6). To generate wide-bandwidth dynamic data or to implement fast control loops, these valves must be capable of responding to high-frequency dynamic signals.

In designing such a servosystem, the designer usually considers the linear dynamics of the electrohydraulic servosystem and finds ways to optimize the linear response through available control-system techniques (ref. 7). However, once the linear dynamics have been extended through compensation, the servosystem becomes limited in its dynamic performance by such nonlinearities as signal saturations or limited available hydraulic power. A previous analysis (refs. 8 and 9) of servosystems containing a two-stage electrohydraulic servovalve was performed to determine the effect that limiting the hydraulic power available to the actuator would have. That analysis derived acceleration and flow limits on the dynamic response of the hydraulic actuator piston for peak-power-transfer operation. Such performance limits are nonlinear and tend to degrade the servoactuator's linear dynamic performance for large-amplitude motions. The relationships that define the limits relate the amplitude and frequency of the output sinusoid. On a log-magnitude-versus-log-frequency plot, these limits are straight lines that define the upper performance bound. This technique has been successfully used to design overboard bypass doors for supersonic inlets (refs. 2 and 3). It has also been used to design a high-response airflow valve for generating upstream airflow perturbations and distortions in a turbojet-engine altitude test chamber (ref. 1).

This report extends the analytical technique derived in reference 9 to the case where a saturating nonlinearity exists in the generation of a position error signal. The system described herein was designed with a single-stage electrohydraulic servovalve consisting of a four-way hydraulic spool valve centered with springs and driven by a high-current coil similar to an audio speaker driver. The single-stage servovalve was intended to provide better linear dynamics than a conventional two-stage servovalve. By using feedback compensation around the spring-mass spool system, the linear frequency response can be extended to the point where system nonlinearities become the major determinant of servosystem dynamic response. In this system, saturation occurs at the output of the power amplifier that drives the coil. Therefore, a technique is needed to readily predict how this saturation affects the system response. Such a technique would also provide a means for selecting such design parameters as spring rate and actuator piston area.

Although the analysis reported herein is used for electrohydraulic servosystems, its application to other servosystems containing saturation is apparent. To provide a more useful approach, this report derives a simple, generalized technique for determining how saturating nonlinearities affect the maximum obtainable frequency response for a typical feedback control system. The analysis derives two lines on the log-amplitude-versus-log-frequency plot that define system operation in the nonlinear region. The first line is determined by assuming that the saturating device puts out a sine

2

wave with a peak amplitude equal to the saturation level and then applying this amplitude to the low- and high-frequency asymptotic approximations of the system dynamics. This line, called the linear-nonlinear transition bound, defines a locus of points where the system initially crosses from total linear operation to operation with saturation. The second line is derived in a similar manner, except that the output of the saturating device is assumed to be a square wave and the amplitude of the square wave's fundamental frequency is applied to the system dynamics. This line, called the maximum-performance limit line, provides a locus of points beyond which system operation is theoretically not possible.

These analyses use asymptotic approximations to system dynamics; therefore, the locations of the bounds defined by these lines may be in error near breakpoints in the asymptotes or at system resonant frequencies. For most systems with well-damped poles, these simple lines are adequate for performance predictions and, as such, provide a very quick and easy approach. However, if the system being analyzed is known to have lightly damped poles, the limit lines must be derived by considering the exact magnitude of the system dynamics at all frequencies. This results in a more complex relationship and a limit-line plot that is not linear on the log-amplitude-versus-log-frequency plot. An example of such a system is provided.

The limit lines (both simple and complex) for the example system are combined with the system linear dynamics in an iterative analysis to determine the system phase-angle response. This results in a family of phase curves with the input command amplitude as the parameter.

The analysis of the example system is presented and compared with an analog computer model. The limit-line technique is then applied to the design of an electrohydraulic servosystem driven by a single-stage servovalve. The saturation technique is used to predict how coil voltage and current saturations affect system dynamic response. These are combined with the actuator velocity and acceleration limits to provide a complete prediction of system performance. The actual servosystem was tested by using frequency sweeps at various commanded amplitudes. The test results are presented in the form of nonnormalized amplitude and phase plots and are compared with the predicted performance.

This work supported the design of a specific actuator. The actuator was used both as a key control element in a stabilizing control system and as a high-frequency perturbation device for dynamic studies. However, the fundamental assumptions and relationships derived should be applicable to any servosystem containing similar nonlinearities.

3

# DERIVATION OF SATURATION PERFORMANCE LIMITS

## Simple Limit Lines for a System with Saturation

To provide a somewhat generalized treatment of a servosystem operating with its error signal in saturation, we analyzed the simplified unity-gain feedback system shown in figure 1. All symbols are defined in appendix A. The error signal E was generated by differencing the command signal R and the output signal C. This error was multiplied by the gain $K_e$ and limited by the saturation block (labeled $K_{nl}$) to provide a force signal F. The system dynamics are represented as a second-order lag with a free integrator and a steady-state gain $K_p$.

To simplify the analysis of the system when it is operating in saturation, we first assumed that only the low-frequency dynamics are important ($|as^2 + bs| < 1$) and then that only the high-frequency dynamics are important ($|as^2| > |bs + 1|$). This resulted in solutions that asymptotically approximate the dynamics of the second-order pole.

Low-frequency linear performance bound. - From figure 1, the transfer function that relates the output to the force for low-frequency dynamics can be written as

$$\frac{C(s)}{F(s)} = \frac{K_p}{s} \tag{1}$$

If the force signal is a sinusoid whose peak amplitude just touches the saturation level (or $|F(s)| = F_{sat}$), letting $s = j\omega$ and taking magnitudes give

$$|C| = \frac{K_p F_{sat}}{\omega} \tag{2}$$

If this relationship is plotted as $|C|$ versus $\omega$ on a log-log plot, the resulting straight line is the dynamic bound between linear and nonlinear operation. Figure 2 presents a plot of this line (the low-frequency segment of the dashed lines) for three values of $K_p$. The numerical parameters chosen for this system are presented in table I.

High-frequency linear performance bound. - The output transfer function for high-frequency dynamics (fig. 1) is

$$\frac{C(s)}{F(s)} = \frac{K_p}{as^3} \tag{3}$$

Again, letting $|F(s)| = F_{sat}$ and $s = j\omega$ give

4

$$|C| = \frac{K_p F_{sat}}{a \omega^3} \tag{4}$$

which is the Bode-plot locus of points for the high-frequency transition from linear to nonlinear operation. These lines are the high-frequency segments of the dashed lines in figure 2. They have a slope of -3 decades per decade; the low-frequency line has a slope of -1 decade per decade.

Limit lines. - Although the previously derived lines are convenient for defining the transition from linear to nonlinear system performance, they do not provide information as to the maximum achievable dynamic performance with this system. Maximum performance is obtained by assuming that the error signal E is at a sufficiently large amplitude to make the saturating-device output F approach a square wave with an amplitude that is set by the saturation level. The fundamental frequency of the square wave is the same as the excitation frequency.

Describing-function theory (refs. 10 and 11) defines the output from a saturating device as

$$f(t) = B_1 \sin \omega t + \sum_{n=3,5,\ldots}^{\infty} B_n \sin n\omega t \tag{5}$$

for an input of

$$K_e e(t) = K_e |E| \sin \omega t \tag{6}$$

where

$$B_1 = \frac{2}{\pi} (K_e |E|) \left[ \sin^{-1}\left(\frac{F_{sat}}{K_e|E|}\right) + \frac{F_{sat}}{K_e|E|} \sqrt{1 - \left(\frac{F_{sat}}{K_e|E|}\right)^2} \right] \tag{7}$$

To approximate this signal, we considered only the fundamental frequency of the force signal $f(t)$. The describing function coefficient $B_1$ was determined by taking the limit of equation (7) as the error-signal amplitude $|E|$ approached infinity.

$$B_1 = \frac{4}{\pi} F_{sat} \tag{8}$$

This gives

$$f(t) = \frac{4}{\pi} F_{sat} \sin \omega t \tag{9}$$

5

Using this input for deriving the plant high- and low-frequency output amplitudes results in

Low-frequency limit:

$$|C| = \frac{4K_p F_{sat}}{\pi \omega} \tag{10}$$

High-frequency limit:

$$|C| = \frac{4K_p F_{sat}}{\pi a \omega^3} \tag{11}$$

The lines defined by equations (10) and (11) represent the maximum output amplitude obtainable for a given frequency. Figure 2 shows the maximum-performance lines (solid) for three values of $K_p$. Essentially, they are the linear-nonlinear transition bounds shifted in magnitude by a factor of $4/\pi$. The region between the dashed and solid lines defines the operating region where the saturating-device output is a clipped sine wave - the nonlinear performance region. In all cases, the low-frequency lines intersect the high-frequency lines at the natural frequency of the second-order pole (100 Hz). The solid lines are referred to as the system-performance limit lines throughout the remainder of the report.

Analog computer model of example system. - To verify the derived limit lines, we implemented the system of figure 1 on an analog computer and subjected it to frequency sweeps with various input-commanded amplitudes $|R|$. The tests were performed with the second-order-pole damping ratio $\zeta$ at 0.7 for the three values of $K_e$ and $K_p$ shown in table I. The product $K_e K_p$ was kept constant to maintain the same closed-loop linear dynamics for all cases.

The results of these tests are shown in figure 3 with the respective limit lines drawn in. System output amplitude $|C|$ is plotted against frequency on a log-log plot. Figure 3(a) ($K_e = 10$, $K_p = 50$) shows that the large-amplitude response ($|R| = 5$) was degraded and followed the limit line for frequencies above 16 hertz. However, when the forward-loop gain $K_e K_p$ was redistributed to place more gain downstream of the saturating device, the limit lines moved up in amplitude and were less of a restriction on large-amplitude performance, as shown in figure 3(b) for gains of $K_e = 5$ and $K_p = 100$. When $K_e$ was decreased to 1 and $K_p$ was increased to 500, the system operated linearly for amplitudes $|R|$ of 0.5, 1.0, and 2.0, as shown in figure 3(c). For all cases shown here, the actual system response was somewhat lower than the limit lines at the 100-hertz natural frequency of the open-loop pole. This prediction error is due to the

6

asymptotic approximations to the second-order-pole dynamics that were used to derive the limit lines.

## Derivation of Complex Limits

The previous derivation used asymptotic approximations to the second-order pole in the plant dynamics. Often a servosystem may contain a lightly damped pole, in which case asymptotes display considerable errors when used to approximate the system dynamics. To analyze such a system, the limit lines must be derived by considering the exact magnitude of the system response at all frequencies.

Analysis of saturation followed by a lightly damped pole. - For the system in figure 1, the transfer function for the dynamics between C and F can be written as

$$\frac{C(s)}{F(s)} = \frac{K_p}{s(as^2 + bs + 1)} \tag{12}$$

If sinusoidal excitations are assumed, $s = j\omega$ can be substituted and the saturating-device output can have a peak amplitude equal to the saturation level ($|F(s)| = F_{sat}$). Then the output amplitude is

$$|C| = \frac{K_p F_{sat}}{\omega \sqrt{a^2 \omega^4 + (b^2 - 2a)\omega^2 + 1}} \tag{13}$$

This relationship defines the linear-nonlinear transition bound, as before, but in a more complex form. Similarly, the maximum-performance limit line is found by assuming the saturating-device output to be a square wave and taking the fundamental-frequency amplitude to be $4/\pi$ times the saturation level. Therefore, the complex limit line is

$$|C| = \frac{4K_p F_{sat}}{\pi \omega \sqrt{a^2 \omega^4 + (b^2 - 2a)\omega^2 + 1}} \tag{14}$$

The complex limit line is plotted in figure 4 for various damping ratios and is compared with the asymptotic limit line for the case where $K_e = 5$ and $K_p = 100$. From this figure, we can conclude that the asymptotes give good results for systems with damping ratios near critical damping but underestimate the response for lightly damped systems and overestimate it for highly damped systems.

Analog computer model of lightly damped example system. - Again, to verify this analysis, we ran a lightly damped case on the analog model. However, when trying to place a lightly damped pole in the forward path of a closed-loop system, it is difficult to

7

close the loop and obtain good relative stability. In a practical system, an attempt is usually made to provide additional damping by closing a velocity feedback loop around the lightly damped pole. The electrohydraulic servosystem to be discussed later is such a system. To provide an analysis relevant to that case, and also to allow for comparison between the $\zeta = 0.2$ and $\zeta = 0.7$ results with the example system, we included a velocity feedback loop, as shown in figure 5. The damping ratio of the second-order pole was set to a damping ratio of 0.2 (P3), and the velocity feedback loop P5 was placed outside the saturation device to create an effective damping ratio of 0.7 when the system operated linearly. Then, when the system went into hard saturation, the loop would be effectively opened and the damping ratio would drop to approach 0.2.

The result of this test is presented in figure 6, along with the complex limit line and the linear-nonlinear transition bound. The large-amplitude responses for $|R|$ of 5 and 9 are relatively flat until they intersect the limit line, after which the response curves follow the limit line closely. The sweep that was done at an amplitude $|R|$ of 2 does not reach the limit line at all. But it does cross the linear-nonlinear transition bound, and the partial saturation distorts the response somewhat from the linear response. In terms of linear dynamics, the system presented in figure 6 is essentially the same as the one presented in figure 3(b). But comparing these two figures shows that the system that has a lightly damped pole following the saturation can extend its large-amplitude response beyond that obtained with a highly damped system. For example, the system response for an $|R|$ of 5 in figure 3(b) is down 3 decibels at a frequency of 43 hertz, but for the response in figure 6 the -3-decibel point is at 103 hertz. This implies that, in designing such a system, lightly damped poles should be placed downstream of the saturating device and that the needed damping should be provided with a velocity feedback loop around the saturating device.


System Phase Response


Often the system to be designed will be used as an element in a larger system. In this case, a phase-response prediction is necessary to determine overall system stability. Saturation creates additional phase beyond that found in linear systems, and the added phase is a function of the system command amplitude. Solving for the phase is difficult since either a piecewise linear model in the time domain or a detailed analog computer model is needed.

Phase determination from limit lines. - This section briefly describes a technique for determining phase in a saturating system. The technique uses the limit-line equations and the system linear dynamics. A more detailed discussion of the technique and its digital implementation and the digital program listings are presented in appendix B.

8

Basically, the technique assumes that the system operates linearly with the saturation characteristic replaced by a gain term, $K_{nl}$. This gain is set to unity for all operating conditions where the system linear output amplitude is less than any one of the limit-line amplitudes at a given frequency. When the linear solution for amplitude, at a given frequency and command amplitude, exceeds any of the limit-line amplitudes, the value of $K_{nl}$ is decremented iteratively until the system output amplitude equals the amplitude of the lowest limit line. The resulting linear system with a decreased forward-loop gain is assumed to be a valid model for the system at that particular command amplitude and frequency. The resulting phase between command signal and output signal is assumed to be the correct system phase at that point.

Analog computer model comparison. - The results for this scheme and the analog model data are presented in figure 7(a) for a damping ratio of $\zeta$ of 0.7 and a plant gain $K_p$ of 100. The solid lines represent the analog-model phase response and the data points are the results from the iterative phase technique. Although the simple limit-line equations used to determine these points were asymptotic approximations, the phase results agree well with the analog response. The additional phase contributions caused by larger amplitude excitations can clearly be seen.

The case for the system with an open-loop damping ratio of 0.2 is shown in figure 7(b). The iterative phase technique in this case used the complex limit-line equation and took into account the effective opening of the velocity feedback loop when the device goes into saturation. Additional detail is provided in appendix B. Again good agreement was obtained between the results of the iterative technique and the analog model.


## Multiple Saturations


As the complexity of a control system increases, the possibility of having several amplifiers or devices that can enter into saturation becomes more likely. If one saturation is predominant, the others can be ignored and the previous analysis can be used. But many times, dynamic elements are present between the saturating devices. Which device enters into saturation first is a function of amplitude and frequency. The previous analysis can be used to determine which device is limiting the system performance at any given operating condition by ignoring all but one of the saturations and solving for its limit lines. The same is done for each saturation in succession. This generates a set of limit lines that can be compared in order to determine the most restrictive limit. As frequency increases, the system may shift from one limit line to another, as in the case of the low- and high-frequency limit lines in figure 2. In all cases, the line that most severely limits system response at a given frequency identifies the device that is in saturation and thus is limiting performance.

No rigorous proof is provided for this superposition theory of limit lines. But, as shown in later sections of this report, this technique does agree well with the experimental results.

## APPLICATION OF LIMIT-LINE TECHNIQUE TO DESIGNING A HIGH-RESPONSE ELECTROHYDRAULIC SERVOSYSTEM

The limit-line technique for saturation was developed because of problems in designing servosystems containing a single-stage electrohydraulic servovalve. This section of the report describes a high-response servosystem, derives a set of performance limit lines based on saturation analysis and power limitations, and compares the experimental results with the predicted dynamic response. The system has both a lightly damped resonance and multiple saturations that must be treated in the analysis.

### Description of Airflow-Valve Servosystem

An airflow valve was designed to provide a variable and controllable orifice area for studying the dynamics and controlling the stability of an axial compressor. A schematic diagram of the actuator servosystem used to control the valve area is shown in figure 8. Since the discussion of this report is limited to the servosystem, the slotted cylinder that forms the airflow-valve moving element is treated merely as a load mass on the actuator piston.

Experimentally, the actuator piston position was measured with a linear variable differential transformer (LVDT). Its output signal was fed into an electronic controller, where it was differenced with a precompensated command signal and a set-point signal. The precompensator, a second-order lead-lag circuit, was used to extend the linear response of the servosystem. The error signal was amplified and applied to a power amplifier that drove the coil on the electrohydraulic servovalve. An internal feedback loop provided current feedback to help extend the amplifier-coil dynamics beyond the resisitive-inductive dynamics of the coil.

The electrohydraulic servovalve is a single-stage, four-way spool valve positioned mechanically by the sum of the forces exerted by the springs at either end of the spool and the current-driven coil. The spool valve opens a port to hydraulic supply and return pressures into the actuator piston chambers in order to position the piston. The second-order dynamics of the spool mass suspended by springs is very lightly damped and requires velocity feedback to remain stable. This feedback is provided by the linear velocity transducer (LVT) mounted at the left end of the servovalve spool in figure 8. The

output signal of the velocity transducer is fed into a feedback compensator, which provides essentially an integral-plus-proportional feedback, to provide added damping and to increase the spring-mass resonant frequency.

A detailed block diagram of the servosystem is provided in figure 9. The system is divided into major elements identified by the dashed lines. The controller is an analog circuit that generates the signals to be fed to the power amplifier. The second-order precompensator is shown acting on the command signal. A slew-rate limiter is used to prevent the compensated command signal from requesting very high velocities at large-amplitude excitations. The slew-rate-limiter output is summed with the actuator position feedback and the set point. The error is multiplied by $K_e$ and fed to the power amplifier. The velocity signal from the servovalve spool $K_{st}\dot{x}_s$ is modified by a band-pass filter to provide a high-pass-filtered and integrated spool velocity signal. This signal allows the spool resonant frequency to be increased without decreasing the steady-state, effective forward-loop gain.

The power amplifier is modeled as a high-gain amplifier $K_{pa}$ whose output $e_{pa}$ can saturate. The power-amplifier voltage output is applied to the first-order lag of the servovalve coil formed by $R_c$ and $L_c$ to generate a coil current $i_c$ that also has a saturation level. This saturation is built into the amplifier as an adjustable limit whose maximum is determined by the coil thermal operating limits. The current is measured by the voltage drop across the series resistor $R_1$ and is fed back into the power amplifier. Since the current-measuring resistor is in series with the coil, the voltage drop across it is subtracted from the power-amplifier output voltage before it is applied to the coil impedance. Coil current passing through the permanent-magnet field $K_c$ creates an excitation force $f_c$ that is differenced with the spring force $K_{sp}x_s$ to accelerate the servovalve spool mass $M_s$. The spring-mass spool mechanical system is modeled as a pure second-order system whose output is spool-valve position $x_s$.

The spool position is the input to the servovalve orifice equations that determine the hydraulic flows and pressures in the actuator cavities (refs. 12 and 13). The spool orifice areas are computed by assuming symmetry and applying an open-center bias area $A_0$. Four orifice equations are used to solve for flows that are applied to the actuator volume dynamics in order to determine the chamber pressures $p_1, p_2$. The pressure difference $p_a$ across the piston accelerates the piston load mass $M_v$, and a double integration provides piston or airflow-valve position $x_v$.

To analyze the dynamic performance limits of this system, we must consider the saturations of the coil voltage $e_{pa}$ and coil current $i_c$, the lightly damped resonances formed by the servovalve spool dynamics ($x_s$ to $f_c$), and the actuator hydraulic volume dynamics ($\dot{x}_v$ to $x_s$). The physical parameters that were used to model the airflow-valve servosystem are listed in table II.

The airflow valve mounted on a test stand is shown in figure 10. The servovalve was rotated 90° relative to its position in figure 8 to prevent case vibrations caused by

piston motion from coupling into the spool position. This could create an instability. The servovalve was attached directly to the actuator block to minimize the hydraulic volume of the actuator control ports.

## Actuator-Piston Acceleration Limit

The limit lines derived in this section and the next are similar to those derived in reference 9 and pertain to the power-drive limitations imposed by the finite supply pressure and flow orifice areas of the servovalve. The load that the actuator piston drives against is assumed to be a pure inertia load set by the mass $M_v$ of the slotted, cylindrical airflow valve and the actuator piston. The force balance on the piston does include a damping term (fig. 9) that is very small relative to the pressure forces and is neglected for this analysis. The resulting equation is

$$M_v \ddot{x}_v = A_a(p_1 - p_2) = A_a p_a \tag{15}$$

The dynamic performance limit for the actuator piston is obtained by assuming that the pressure drop across the piston is at its peak value. Under ideal circumstances, the maximum force available to accelerate the actuator piston is estimated by assuming one chamber to be at full supply pressure $P_{su}$ and the other chamber to be at zero pressure. However, a better approximation to peak pressure is obtained by assuming the piston pressure-flow characteristics to be operating on an ellipse that delivers peak power to the actuator. A complete derivation of this curve and the resulting peak pressures and flows are presented in appendix C. The resulting peak pressure is

$$p_{a, \, peak} = \frac{2}{3} \sqrt{2} \, P_{su} \tag{16}$$

Assuming sinusoidal output motion ($x_v = |X_v| \sin \omega t$) and equating peak values for equation (15) give

$$|X_v| \omega^2 = \frac{2\sqrt{2} \, A_a P_{su}}{3M_v} \tag{17}$$

which is the expression for the actuator acceleration limit.

12

## Actuator Piston Velocity Limit

The actuator piston velocity is essentially proportional to the hydraulic flow entering the piston chambers. If the fluid is incompressible,

$$q_3 = q_6 = q_s \tag{18}$$

Based on this assumption, the flow balance for one volume of the actuator piston chamber would be

$$q_s = A_a \dot{x}_v \tag{19}$$

The maximum possible velocity is determined from the maximum servovalve flow. To find what the maximum flow would be, we use the peak-power elliptical load line of appendix C. That is,

$$(q_s)_{peak} = \sqrt{2}\, Q_r \tag{20}$$

where $Q_r$ is the servovalve rated flow at the peak-power transfer point and is defined as the flow through the servovalve orifices when the load pressure on the piston is

$$p_a = \frac{2}{3} P_{su} \tag{21}$$

and the spool valve is at its maximum open condition. The flow through the servovalve orifices for a positive displacement of $x_s$ can be written as

$$q_3 = \pi d_s x_s C_d \sqrt{\frac{2}{\rho}(P_{su} - p_1)} \tag{22}$$

$$q_6 = \pi d_s x_s C_d \sqrt{\frac{2}{\rho} p_2} \tag{23}$$

From equation (18) we can set equation (22) equal to equation (23) to get

$$P_{su} = p_1 + p_2 \tag{24}$$

Using the assumption of matched symmetrical orifices, we derive the following relationship for flow:

$$q_s = \pi d_s x_s C_d \sqrt{\frac{1}{\rho}(P_{su} - p_a)} \tag{25}$$

13

(ref. 12, pp. 81-83). Substituting equation (21) into equation (25) gives the rated flow

$$Q_r = \pi d_s |X_s|_{max} C_d \sqrt{\frac{P_{su}}{3\rho}} \tag{26}$$

where $|X_s|_{max}$ is the maximum spool displacement amplitude.

Substituting equations (20) and (26) into equation (19) and considering only amplitudes give

$$|X_v|\omega = \frac{K_l |X_s|_{max}}{A_a} \tag{27}$$

where

$$K_l = \pi d_s C_d \sqrt{\frac{2P_{su}}{3\rho}} \tag{28}$$

This equation is the velocity limit for the airflow-valve servosystem. However, the maximum displacement of the servovalve spool is not a constant value. It depends on the saturation levels of the current and voltage signals that drive the spool coil. The term $K_l$ can be viewed as the linearized gain between the spool position and the serovalve flow.

Coil-Current Limit

From the block diagram of figure 9, we can write the transfer function for servo-valve spool position to coil current as

$$\frac{X_s(s)}{I_c(s)} = \frac{\dfrac{K_c}{K_{sp}}}{\dfrac{M_s}{K_{sp}}s^2 + \dfrac{D_s}{K_{sp}}s + 1} \tag{29}$$

For only low frequencies,

$$\frac{X_s(s)}{I_c(s)} = \frac{K_c}{K_{sp}} \tag{30}$$

14

Assuming a sinusoidal coil current whose peak amplitude is at the saturation level and considering only magnitudes give

$$|X_s| = \frac{K_c}{K_{sp}} I_{c,sat} \tag{31}$$

which is the spool displacement amplitude at which the system crosses the linear-nonlinear performance bound. As was shown earlier, the maximum possible spool displacement at low frequencies is given by

$$|X_s|_{max} = \frac{4K_c I_{c,sat}}{\pi K_{sp}} \tag{32}$$

Substituting equation (32) into equation (27) gives the low-frequency coil-current limit.

$$|X_v| \omega = \frac{4K_l K_c I_{c,sat}}{\pi K_{sp} A_a} \tag{33}$$

Returning to equation (29) and considering only high frequencies yield

$$\frac{X_s(s)}{I_c(s)} = \frac{K_c}{M_s s^2} \tag{34}$$

Substituting $s = j\omega$, taking magnitudes, and letting $|I_c(s)| = I_{c,sat}$ give

$$|X_s| \omega^2 = \frac{K_c}{M_s} I_{c,sat} \tag{35}$$

for current peaks at the saturation level. Solving for $|X_s|$, applying the $4/\pi$ factor, and substituting into equation (27) give the high-frequency coil-current limit.

$$|X_v| \omega^3 = \frac{4K_l K_c I_{c,sat}}{\pi M_s A_a} \tag{36}$$

Coil-Voltage Limit

The presence of coil-current saturation is ignored in this section, and the effect of coil-voltage saturation is investigated. The linear transfer function between the spool

15

position and the coil voltage includes the dynamics of the servovalve coil and the spring-mass dynamics of the spool. Since this analysis treats the case of saturation, the spool velocity feedback loop is assumed to be effectively open. The transfer function is

$$\frac{X_s(s)}{E_{pa}(s)} = \frac{\dfrac{K_c}{K_{sp}(R_1 + R_c)}}{\left(\dfrac{M_s}{K_{sp}} s^2 + \dfrac{D_s}{K_{sp}} s + 1\right)\left(\dfrac{L_c}{R_1 + R_c} s + 1\right)} \tag{37}$$

Assuming only low frequencies gives

$$\frac{X_s(s)}{E_{pa}(s)} = \frac{K_c}{K_{sp}(R_1 + R_c)} \tag{38}$$

If we use the same techniques as in the previous section, the low-frequency limit line becomes

$$\left|X_v\right| \omega = \frac{4K_l K_c E_{pa,\,sat}}{\pi K_{sp}(R_1 + R_c)A_a} \tag{39}$$

Similarly, the high-frequency transfer function is

$$\frac{X_s(s)}{E_{pa}(s)} = \frac{K_c}{M_s L_c s^3} \tag{40}$$

and the high-frequency coil-voltage limit line is

$$\left|X_v\right| \omega^4 = \frac{4K_l K_c E_{pa,\,sat}}{\pi M_s L_c A_a} \tag{41}$$

The limit-line equations for the airflow-valve servosystem were determined from the parameters of table II and are presented in table III in summary form. Figure 11 provides a plot of these equations, showing the linear-nonlinear transition bounds as dashed lines and the maximum-performance limit lines as solid lines. The coil-voltage limits are beyond the coil-current limits for almost all frequencies and, therefore, they are only a factor for frequencies beyond 900 hertz. The acceleration limit line is located just beyond the coil-current limit lines.

## Using Limit Lines to Design the System

Inspection of the limit-line equations of table III reveals that a common parameter is actuator piston area $A_a$. By selecting this area, the position of the limit lines can be selected. The magnitude of the acceleration limit line is a direct function of piston area, but the coil current and voltage limits vary inversely with piston area. The movement of a typical set of coil-current and acceleration limit lines for decreasing piston area is shown in figure 12. The coil-current lines move up in amplitude and frequency while the acceleration limit line moves down. To select a piston area that would tend to maximize the system response, we equate the point where the low- and high-frequency current-limit lines intersect with the acceleration limit line.

The intersection of low- and high-frequency current limits is found from

$$|X_v| = \frac{4K_l K_c I_{c,sat}}{\pi K_{sp} A_a \omega} = \frac{4K_l K_c I_{c,sat}}{\pi M_s A_a \omega^3} \tag{42}$$

which results in

$$\omega^* = \sqrt{\frac{K_{sp}}{M_s}} \tag{43}$$

which, of course, is the resonant frequency of the spring-mass spool dynamics. Evaluating the acceleration limit at the frequency defined in equation (43) gives

$$|X_v| = \frac{4K_l K_c I_{c,sat}}{\pi M_s A_a^* \left(\dfrac{K_{sp}}{M_s}\right)^{3/2}} = \frac{2\sqrt{2}\, A_a^* P_{su} M_s}{3 M_v K_{sp}} \tag{44}$$

or solving for $A_a^*$

$$A_a^* = \left(\frac{3\sqrt{2}\, K_l K_c I_{c,sat} M_v}{\pi P_{su} \sqrt{M_s K_{sp}}}\right)^{1/2} \tag{45}$$

which is the actuator area that will make the limit lines intersect, as shown by the dashed lines in figure 12. From the parameters in table II, the optimum area is 2.96 square centimeters. The actual area used, 3.20 square centimeters, was a design compromise based on piston-seal sizing considerations. We decided to use a larger than optimum area because this made the coil-current limit the predominant limit. Since the

dynamics downstream of the current saturation contained a lightly damped resonance, the actual system response will probably exceed the coil-current limit line near the resonance.

## Complex Limit Lines for Airflow-Valve Servosystem

As was discussed in earlier sections, the presence of lightly damped poles downstream of the saturating device requires a more exact solution for the limit lines, one that uses transfer-function magnitudes rather than asymptotes. Figure 9 shows that, besides the resonance of the servovalve spool spring-mass, there exists a second-order resonance formed by the stiffness of the hydraulic fluid $\beta$ driving the piston mass $M_v$. This resonance was ignored when the limit lines were derived because the actuator volumes and the piston and airflow-valve masses were sized to set this resonant frequency beyond the range of interest. However, practical design considerations lowered the resonant frequency to 472 hertz, which is near the 315-hertz resonance of the servovalve spool. Therefore, when the transfer function used to derive the complex limit lines is being written, the piston hydraulic resonance should also be considered, as shown by the simplified block diagram of figure 13.

The following derivation will be carried out for the coil-current limit since it is the most restrictive of the saturating limits. The coil-voltage limit could be determined similarly by including the coil impedance between $e_{pa}$ and $i_c$.

The original derivation of the actuator velocity limit basically used the same block diagram with the transfer function of $x_v$ to $q_s$ replaced by $1/A_a s$. The transfer function from $I_c(s)$ to $X_v(s)$ can be written as

$$\frac{X_v(s)}{I_c(s)} = \frac{\dfrac{K_c K_l}{K_{sp} A_a}}{s\left(\dfrac{M_s}{K_{sp}} s^2 + \dfrac{D_s}{K_{sp}} s + 1\right)\left(\dfrac{V_t M_v}{4\beta A_a^2} s^2 + \dfrac{K_{fp,0} M_v}{\sqrt{2} A_a} s + 1\right)} \tag{46}$$

The spool flow to pressure gain $K_{fp,0}$ was determined from the relationship in reference 12 (p. 97). The denominator terms can be simplified by rewriting them in natural frequency and damping ratio form

$$\frac{X_v(s)}{I_c(s)} = \frac{\dfrac{K_c K_l}{K_{sp} A_a}}{s\left(\dfrac{1}{\omega_{ns}^2} s^2 + \dfrac{2\zeta_s}{\omega_{ns}} s + 1\right)\left(\dfrac{1}{\omega_{nh}^2} s^2 + \dfrac{2\zeta_h}{\omega_{nh}} s + 1\right)} \tag{47}$$

where

$$\omega_{ns} = \sqrt{\frac{K_{sp}}{M_s}} \tag{48}$$

$$\zeta_s = \frac{D_s}{2\sqrt{K_{sp} M_s}} \tag{49}$$

$$\omega_{nh} = 2A_a \sqrt{\frac{\beta}{V_t M_v}} \tag{50}$$

$$\zeta_h = \frac{K_{fp,0}}{2A_a} \sqrt{\frac{2\beta M_v}{V_t}} \tag{51}$$

Assuming the input $i_c$ to be the fundamental component of a square wave and the output $x_v$ to be a sine wave with a zero-to-peak amplitude of $\left| X_v \right|$ and taking the magnitude of the transfer function by replacing $s$ with $j\omega$ give

$$\left| X_v \right| \omega = \frac{\dfrac{4K_l K_c I_{c,sat}}{\pi K_{sp} A_a}}{\left| \left[1 - \left(\dfrac{\omega}{\omega_{ns}}\right)^2\right] + j2\zeta_s\left(\dfrac{\omega}{\omega_{ns}}\right) \right| \times \left| \left[1 - \left(\dfrac{\omega}{\omega_{nh}}\right)^2\right] + j2\zeta_h\left(\dfrac{\omega}{\omega_{nh}}\right) \right|} \tag{52}$$

which is the equation for the complex coil-current limit line. The limit line is plotted in the following section for the airflow-valve servosystem.

## RESULTS AND DISCUSSION

Experimental data for the dynamic response of the airflow-valve servosystem were obtained by sweep frequency-response techniques at various excitation amplitudes. The

frequency responses were plotted with the log of nonnormalized amplitude on the vertical axis and the log of frequency on the horizontal axis. The results are shown in figure 14 for excitation amplitudes of 5, 10, 20, 40, 80, and 100 percent of full stroke (full stroke = 0.318 cm, zero to peak). For comparison, the acceleration limit line and the complex current-saturation limit line are plotted on this figure. The amplitude response of the servosystem moving a 1.1-kilogram mass was flat to within 3 decibels of the low-frequency amplitude to 530 hertz for a 20-percent amplitude signal. This response degraded to 200 hertz for an 80-percent amplitude signal.

The output was limited at large amplitudes by the slew-rate limiter used to precompensate the command signal in order to avoid excessive velocities. At frequencies between 300 and 550 hertz, the system resonated through the current limit asymptotes to the acceleration limit line. For frequencies beyond 550 hertz the amplitude dropped off along the complex current limit line. This amplitude result agrees well with the predicted performance derived from the limit-line analysis. The small-amplitude response at 10-percent amplitude is essentially the linear response of the system for frequencies to about 600 hertz. At 5-percent amplitude, stiction tends to decrease the resonant peak.

Figure 15 presents the phase response of the airflow-valve servosystem for 20- and 100-percent excitation amplitudes. The system crossed the $-90^\circ$ point at 270 and 140 hertz for 20- and 100-percent amplitudes, respectively. The data points shown on the curves are the phase prediction from the iterative analysis that was based on the presence of the acceleration limit and the complex current limit line. The slew-rate limiter was also modeled to achieve agreement with the 100-percent-amplitude result.


CONCLUSIONS


An analysis for determining the dynamic response limitations for a servosystem containing saturations has been presented for a simple second-order system and for a practical electrohydraulic servosystem design. The boundary between linear and nonlinear performance is determined for saturation by assuming a peak amplitude out of the saturating device equal to the saturation level and by applying this amplitude to the linear dynamics between the saturating device and the system output. The maximum-performance limit line is the same as the nonlinear bound line, but with the system output amplitude multiplied by $4/\pi$.

Having applied the limit-line criteria to these systems, we can draw the following conclusions:

1. When designing a system with saturation, it is desirable to distribute as much of the forward-loop gain as possible downstream of the saturating device.

2. The use of asymptotes to approximate linear performance is reasonable for systems with damping ratios of 0.5 to 1.0. However, systems with lightly damped, open-

loop poles downstream of the saturation may require a more detailed analysis near the resonant frequency. This analysis shows that the system performance can exceed the asymptotic maximum-performance limit line because of the system's high gain at the resonant frequency.

3. Decreasing the damping on the open-loop pole and creating the needed damping by using a feedback loop around the limiting device can extend the response of a system near the open-loop resonant frequency. This technique results in a response somewhere between the asymptotic limit lines and the detailed complex limit line.

4. For systems with more than one saturation, the limit lines can be obtained by treating one saturation at a time and assuming the other saturating devices to be in their linear operation regions. The most restrictive limits are then used to define the maximum-performance region.

5. The optimum actuator piston area for an electrohydraulic servosystem can be determined from the limit-line equations to provide the maximum system performance.

6. If the design specifications for a servosystem stipulate maximum allowable velocities or accelerations, parameters can be chosen to position the limit lines to assure that these specifications are not exceeded.

The iterative technique of combining the predominant limit lines with the system linear response to determine system output phase response provides good agreement with actual system response. The assumption that operating in saturation opens any feedback loops around the saturating device is an oversimplification that may require further investigation. Since the linear feedbacks are functional over the portion of the waveform period when zero-error crossover occurs, a modified set of relationships could be developed to treat this case. Although the scope of this work precluded entering into this type of detail, it is suggested for future studies.

The fast-response electrohydraulic servosystem designed with the limit-line technique provided good dynamic response. It moved a mass of 1.1 kilograms through a peak-to-peak displacement of 0.127 centimeter at 530 hertz ($\pm3$ dB), with a phase angle of $-90°$ at 270 hertz. This response agreed well with the predicted results from the limit-line analysis.

Lewis Research Center,
    National Aeronautics and Space Administration,
        Cleveland, Ohio, March 30, 1979,
            505-05.

# APPENDIX A

## SYMBOLS

A      area, $cm^2$

a      example-system transfer-function coefficient, $sec^2$

B      describing-function coefficient (pseudo force signal)

b      example-system transfer-function coefficient, sec

C      orifice discharge coefficient

C(s)      example-system output signal (frequency domain)

c      example-system output signal (time domain)

D      damping factor, $N \cdot sec/cm$

d      diameter, cm

E(s)      example-system error signal (frequency domain)

e      airflow-valve servosystem voltage, V

e(t)      example-system error signal (time domain)

F      force level, N

F(s)      example-system pseudo force signal (frequency domain)

f(t)      force (time domain), N

I(s)      current (frequency domain), A

i      current (time domain), A

K      gain

$K_c$      servovalve coil-force-to-coil-current gain, N/A

$K_{fp,0}$      servovalve null flow-pressure coefficient, $cm^5/N \cdot sec$

$K_l$      servovalve linearized flow to maximum spool position for peak-power transfer point, $cm^2/sec$

$K_{pa}$      power amplifier gain, V/A

$K_{sp}$      spring rate, N/cm

$K_{ps}$      proportional gain for spool velocity feedback, V/V

$K_{is}$      integral gain for spool velocity feedback, $sec^{-1}$

$K_{st}$      spool velocity transducer gain, $V \cdot sec/cm$

$K_{vt}$     airflow-valve position transducer gain, V/cm

L        inductance, H

M        mass, $N \cdot sec^2/cm$

P        pressure (steady state), $N/cm^2$

p        pressure (instantaneous), $N/cm^2$

Q        volumetric flow (steady state), $cm^3/sec$

q        volumetric flow (instantaneous), $cm^3/sec$

R        resistor, $\Omega$

R(s)     example-system input command signal (frequency domain)

r(t)     example-system input command signal (time domain)

s        Laplace operator, 1/sec

T        sine-wave period, sec

t        time, sec

X(s)     position (frequency domain), cm

x        position (time domain), cm

V        volume, $cm^3$

$\beta$     bulk modulus, $N/cm^2$

$\zeta$     damping ratio

$\rho$     hydraulic fluid density, $N \cdot sec^2/cm^4$

$\tau$     time constant, sec

$\omega$     frequency, rad/sec

$|\ |$     zero-to-peak amplitude of sinusoid

Subscripts:

A        peak-power point

a        actuator

c        coil

cc       command compensator

cl       closed loop

com      command

d        discharge

23

| | |
|---|---|
| e | error |
| eff | effective |
| full | full stroke |
| h | hydraulic |
| max | maximum |
| n | numbers in sequence |
| nl | saturating nonlinear device |
| nh | hydraulic natural frequency |
| ns | servovalve-spool natural frequency |
| ol | open loop |
| p | plant |
| pa | power amplifier |
| peak | peak amplitude |
| pre | precompensated command |
| r | rated |
| s | spool |
| sat | saturation |
| set | set point |
| su | supply |
| t | total |
| v | airflow valve |
| 0 | null |
| 1,2... | numerical subscripts used as noted in text |

Superscripts:

| | |
|---|---|
| $(\ )^*$ | optimum |
| $(\dot{\ })$ | first derivative with respect to time |
| $(\ddot{\ })$ | second derivative with respect to time |
| $(\tilde{\ })$ | high-pass-filtered signal |

24

# APPENDIX B

## ITERATIVE PHASE DETERMINATION FROM LIMIT LINES

Once the limit lines for a particular system design have been determined, the phase response of that system can be approximated by combining the limit-line equations with the system linear dynamics. Basically, the system is treated as a linear system with the saturating device replaced by a linearized gain $K_{nl}$. In the linear operating region, $K_{nl}$ is set to 1. When the system is operating in saturation, the effective gain of the saturating device is reduced ($K_{nl} < 1$).

The actual value of $K_{nl}$ is determined by allowing the system output amplitude to equal the limit-line amplitude at that frequency and solving the linear transfer function for $K_{nl}$. Since this will always result in a $K_{nl}$ below 1.0, the solution is implemented by an iterative process. That is, $K_{nl}$ is initialized at 1.0 and is decreased in increments until the linear-transfer-function magnitude equals the most restrictive limit-line magnitude at the selected frequency. The resulting linear transfer function is assumed to be correct, and the phase angle of the system at that particular gain and frequency is assumed to be the system phase response. This procedure results in a system gain that is a function of frequency and input excitation amplitude.

The closed-loop linear transfer function for the example system of figure 1 is

$$\frac{C(s)}{R(s)} = \frac{K_{nl}K_pK_e}{as^3 + bs^2 + s + K_{nl}K_pK_e} \tag{B1}$$

The computer listing that was used to determine the phase plots of figure 7(a) is shown here.

```
C       ITERATIVE PHASE TECHNIQUE
C       PROGRAM #1 - ASYMPTOTIC LIMIT LINES FOR EXAMPLE SYSTEM
        REAL KE,KP,KNL,MAGC
        PI=3.1415926
        WN=2.*PI*100.
        WI=2.*PI*5.
        DELTW=WI
1       WRITE(6,23)
        READ(5,2)KE,KP,FSAT,R,ZETA
        WRITE(7,21)
2       FORMAT(5F8.4)
        W=WI
3       D=W/WN
        KNL=1.
        CMAG=R*KNL*KP*KE/SQRT((KNL*KP*KE-2.*ZETA*D*W)**2+W*W*(1.-D*D)**2)
        IF(W-WN)4,6,6
```

```
4       CLL=(4./PI)*KP*FSAT/W
        GO TO 8
6       CLL=(4./PI)*KP*FSAT/(W*D*D)
8       IF(CMAG-CLL)10,10,12
10      GO TO 14
12      MAGC=R*KNL*KP*KE/SQRT((KNL*KP*KE-2.*ZETA*D*W)**2+W*W*(1.-D*D)**2)
        IF(ABS(MAGC-CLL).LT..01)GO TO 14
        KNL=KNL-.0001
        GO TO 12
14      THETA=-(ATAN2(W*(1.-D*D),(KNL*KP*KE-2.*ZETA*D*W)))
        THETAD=THETA*360./(2.*PI)
        F=W/(2.*PI)
        WRITE(7,16)F,THETAD,CMAG,CLL,KNL
        W=W+DELTW
16      FORMAT(1X,6F12.6)
        IF(F-300.)3,3,18
18      WRITE(6,20)
        READ(5,22)I
20      FORMAT(1X,' RUN ANOTHER CASE? 1=YES,0=NO ')
21      FORMAT(1X,4X,'FREQ',7X,'THETA',9X,'MAG',9X,'CLL',10X,'KNL')
22      FORMAT(I1)
        IF(I)24,24,1
23      FORMAT(1X,' INPUT KE,KP,FSAT,R,ZETA ')
24      STOP
        END
```

The iterative phase technique is not quite as straightforward when used with a lightly damped system containing a velocity feedback loop (figs. 6 and 7(b)). When the system operates linearly, the velocity feedback increases the damping of the forward-loop transfer function. But when the system operates in saturation, this feedback is opened during the saturation portion of the cycle.

The portion of the cycle when the system is in saturation can be found by solving for the time at which the error-signal sine wave reaches saturation or

$$K_e|E| \sin \omega t_1 = F_{sat} \tag{B2}$$

Solving for $t_1$ gives

$$t_1 = \frac{1}{\omega} \sin^{-1}\left(\frac{F_{sat}}{K_e|E|}\right) \tag{B3}$$

If the saturation is assumed to be well established, or $F_{sat}/(K_e|E|) < 0.5$, the approximation

$$\sin^{-1}\left(\frac{F_{sat}}{K_e|E|}\right) \cong \frac{F_{sat}}{K_e|E|} \tag{B4}$$

26

is used to simplify equation (B3), giving

$$t_1 = \frac{F_{sat}}{\omega K_e |E|} \tag{B5}$$

In terms of the sine-wave period, $\omega$ can be replaced by $2\pi/T$. Since $t_1$ is the time from $t = 0$ to the point where the first saturation occurs, there will be four of these time periods in a cycle. The ratio of the time in linear performance to the period of the sine wave is

$$\frac{4t_1}{T} = \frac{2F_{sat}}{\pi K_e |E|} \tag{B6}$$

To estimate the damping ratio for a system with a velocity loop that is closed only a portion of the time, we assume a simple straight-line relationship for the damping ratio.

$$\zeta_{eff} = \zeta_{ol} + (\zeta_{cl} - \zeta_{ol})K \tag{B7}$$

The proportionality constant $K$ is related to the degree of saturation and varies from 1.0 for no saturation to 0 for saturation over the entire period. Equation (B6) defines the percentage of time that the system is not in saturation and is used to give an approximate value for $K$. Therefore,

$$\zeta_{eff} = \zeta_{ol} + (\zeta_{cl} - \zeta_{ol})\left(\frac{2F_{sat}}{\pi K_e |E|}\right) \tag{B8}$$

This equation provides a good approximation for the effective damping ratio resulting from the velocity feedback loop with the system in partial saturation. However, without an exact time-solution at all frequencies, it is difficult to determine the value of $|E|$. It is approximated by a value of $|R|/2$, which was found to give good agreement when used to predict the phase of the lightly damped example-system case. Therefore, the relationship used to determine the effective damping ratio of the forward-loop transfer function for partial saturation is

$$\zeta_{eff} = \zeta_{ol} + (\zeta_{cl} - \zeta_{ol})\left(\frac{4F_{sat}}{\pi K_e |R|}\right) \tag{B9}$$

This damping ratio is switched in when the linear response crosses the limit line before the saturation gain is decremented. A listing for the program used to generate the data of figure 7(b) is presented here.

```
C       ITERATIVE PHASE TECHNIQUE
C       PROGRAM #2 - COMPLEX LIMIT LINE FOR EXAMPLE SYSTEM
        REAL KE,KP,KNL,MAGC
        PI=3.1415926
1       WRITE(6,23)
        READ(5,2)WN,WI,DELTW,KE,KP,FSAT,R,ZETOL
        WRITE(7,21)
2       FORMAT(8F8.4)
        DK=.1
        W=WI
3       D=W/WN
        KNL=1.
        CMAG=R*KNL*KP*KE/SQRT((KNL*KP*KE-2.*.7*D*W)**2+W*W*(1.-D*D)**2)
        DLL=KP*FSAT/(W*SQRT(D*D*D*D+4.*D*D*.04-2.*D*D+1.))
        CLL=DLL*4./PI
        IF(CMAG-CLL)5,5,10
5       ZETA=.7
        GO TO 15
7       ZETA=ZETA+.01
        GO TO 12
10      ZETA=ZETAOL+(ZETA-ZETAOL)*(FSAT*4.)/(KE*R*PI)
12      MAGC=R*KNL*KP*KE/SQRT((KNL*KP*KE-2.*ZETA*D*W)**2+W*W*(1.-D*D)**2)
        IF(ABS(MAGC-CLL).LT..01)GO TO 15
        IF(MAGC-CLL)13,15,14
13      IF(KNL.EQ.1.)GO TO 7
        KNL=KNL+DK
        DK=DK/2
        GO TO 12
14      KNL=KNL-DK
        GO TO 12
15      THETA=-(ATAN2(W*(1.-D*D),(KNL*KP*KE-2.*ZETA*D*W)))
        THETAD=THETA*360./(2.*PI)
        F=W/(2.*PI)
        WRITE(7,16)F,THETAD,CMAG,CLL,KNL,MAGC,ZETA
        W=W+DELTW
16      FORMAT(1X,7F12.6)
        IF(F-300.)3,3,18
18      WRITE(6,20)
        READ(5,22)I
20      FORMAT(1X,' RUN ANOTHER CASE? 1=YES,0=NO ')
21      FORMAT(1X,4X,'FREQ',7X,'THETA',8X,'CMAG',8X,'CLL',9X,'KNL',9X,'MAG-
       1C',10X,'ZETA')
22      FORMAT(I1)
        IF(I)24,24,1
23      FORMAT(1X,' INPUT WN,WI,DELTW,KE,KP,FSAT,R,ZETAOL ')
24      STOP
        END
```

# APPENDIX C

## DERIVATION OF PEAK-POWER EQUATIONS

The peak-power level delivered to a hydraulic actuator piston was determined in reference 9. The derivation of the peak-power ellipse and the resulting theoretical peak values of flow and pressure are repeated here for completeness.

The output, or load acceleration, can be expressed in terms of the pressure across the piston. Substituting $x_v = |X_v| \sin \omega t$ into equation (15) and rearranging result in

$$\frac{A_a}{M_v} P_a(t) = -|X_v| \omega^2 \sin \omega t \tag{C1}$$

where

$$p_a(t) = p_1(t) - p_2(t) \tag{C2}$$

When equation (19) is used, the output velocity can be expressed in terms of the servo-valve output flow as follows:

$$\frac{q_s(t)}{A_a} = |X_v| \omega \cos \omega t \tag{C3}$$

Rearranging equations (C1) and (C3) results in the following two equations:

$$\frac{q_s(t)}{A_a |X_v| \omega} = \cos \omega t \tag{C4}$$

$$\frac{A_a p_a(t)}{M_v |X_v| \omega^2} = -\sin \omega t \tag{C5}$$

Therefore, for sinusoidal motion of the output $x_v(t)$, equations (C4) and (C5) show that the servovalve output spool flow $q_s(t)$ and pressure $p_a(t)$ must also be sinusoidal but with a specific phase relation. Figure 16 is a typical plot of the phase relation of the variables $x_v(t)$, $q_s(t)$, and $p_a(t)$. The valve flow $q_s(t)$ leads the output by $\pi/2$ radians, and the flow and pressure are out of phase by $\pi/2$ radians. When the flow and pressure for one complete sine wave are crossplotted on a servovalve characteristic, a load locus is generated. An expression for this load locus is now derived.

Squaring both sides of equations (C4) and (C5) and adding the results yield

$$\frac{q_s^2}{A_a^2 |X_v|^2 \omega^2} + \frac{A_a^2 p_a^2}{M_v^2 |X_v|^2 \omega^4} = 1 \qquad (C6)$$

Equation (C6) describes an ellipse and represents the locus that would appear on a servovalve output characteristic plot of flow versus pressure for sinusoidal motion of the actuator output position $x_v(t)$.

The largest possible ellipse must be bounded by the maximum spool displacement $\pm |X_s|_{max}$ and the maximum piston pressures $\pm |P_a|_{max}$. To get the most out of the system, the ellipse described by equation (C6) must lie within this region but be tangent to the $\pm |X_s|_{max}$ curves at some point. The choice of this tangent point is somewhat arbitrary but will be selected as the point where the servovalve transfers maximum power to the load. This point is designated as point A in figure 17. The derivation of this point is considered in reference 12 and, therefore, only the results are presented here. The pressure $p_a$ and flow $q_s$ at this peak-power point are as follows:

$$p_{a,A} = \frac{2}{3} P_{su} \qquad (C7)$$

$$q_{s,A} = Q_r \qquad (C8)$$

where $Q_r$ is defined as the servovalve rated flow that normally appears in the specifications. Rated flow is conventionally defined as the maximum flow available from the valve with $(2/3)P_{su}$ across the load.

The derivation for the load locus or ellipse that is tangent to the $|X_s|_{max}$ curve at point A of figure 17 is now presented. The expression for the servovalve pressure-flow characteristic at maximum spool displacement $|X_s|_{max}$ is as follows:

$$q_s = C_s |X_s|_{max} \sqrt{P_{su} - p_a} \qquad (C9)$$

where

$$C_s = \pi d_s C_d \sqrt{\frac{1}{\rho}} \qquad (C10)$$

The generalized expression for the pressure and flow output requirements during sinusoidal output motion is given by equation (C6). After rearranging, this equation becomes

$$q_s^2 = \omega^2 |X_v|^2 A_a^2 - p_a^2 \left( \frac{A_a^4}{M_v^2 \omega} \right) \tag{C11}$$

To determine a specific expression of the load ellipse that is tangent to the servovalve characteristic at point A (fig. 17), we determined and equated the derivatives $dq_s/dp_a$ of equations (C9) and (C11). The result is

$$\frac{C_s |X_s|_{max}}{2 \sqrt{P_{su} - p_a}} = \frac{p_a}{q_s} \left( \frac{A_a^2}{M_v^2 \omega^2} \right) \tag{C12}$$

Substituting $q_s = C_s |X_s|_{max} \sqrt{P_{su} - p_a}$ and rearranging give

$$\frac{q_s}{2(P_{su} - p_a)} = \frac{p_a}{q_s} \left( \frac{A_a^4}{M_v^2 \omega^2} \right) \tag{C13}$$

Substituting in the coordinates of point A of figure 17 $((2/3)P_{su}, Q_r)$ yields an expression for $\omega_A$, the frequency of oscillation for the output locus that passes through point A:

$$\omega_A = \frac{\frac{2}{3} P_{su} A_a^2}{M_v Q_r} \tag{C14}$$

Substituting equation (C14) into equation (C11) at the coordinates of point A yields the peak displacement $|X_{v,A}|$ for the locus through point A:

$$|X_{v,A}| = \frac{3\sqrt{2}\, Q_r^2 M_v}{2 A_a^3 P_{su}} \tag{C15}$$

Substituting equations (C14) and (C15) into the general expression of equation (C11) yields the expression for the maximum output (load) pressure and flow locus:

$$q_s^2 = 2Q_r^2 - p_a^2 \left(\frac{9Q_r^2}{4P_{su}^2}\right) \qquad \text{(C16)}$$

Rearranging yields the following:

$$\frac{q_s^2}{2Q_r^2} + p_a^2 \left(\frac{9}{8P_{su}^2}\right) = 1 \qquad \text{(C17)}$$

This is the expression for the load locus or ellipse that is tangent to the $\left|X_s\right|_{max}$ curve at point A in figure 17. In terms of supply pressure $P_{su}$ and rated flow $Q_r$, its intercepts with $p_a$ and $q_s$ axes are as follows:

$$p_{a,\,peak} = \frac{2}{3}\sqrt{2}\; P_{su} \qquad \text{(C18)}$$

$$q_{s,\,peak} = \sqrt{2}\; Q_r \qquad \text{(C19)}$$

These are the peak piston pressure and flow that the servovalve must supply to enable the output load to generate the locus of equation (C17) when the system is operating in a sinusoidal manner. The values of peak pressure and flow defined by equations (C18) and (C19) then determine the output acceleration and velocity limit criteria, respectively.

# REFERENCES

1. Baumbick, Robert J.: Device for Producing Dynamic Distortion Patterns at Inlets of Air-Breathing Engines. NASA TM X-2026, 1970.

2. Neiner, George H.: Servosystem Design of a High-Response Slotted-Plate Overboard Bypass Valve for a Supersonic Inlet. NASA TN D-6081, 1970.

3. Webb, John A., Jr.; Mehmed, Oral; Hiller, Kirby W.: Improved Design of a High-Response Slotted Plate Overboard Bypass Valve for Supersonic Inlets. NASA TM X-2812, 1973.

4. Baumbick, Robert J.; et al.: Dynamic Response of Mach 2.5 Axisymmetric Inlet with 40 Percent Supersonic Internal Area Contraction. NASA TM X-2833, 1973.

5. Milner, Edward J.; Wenzel, Leon M.; and Paulovich, Francis J.: Frequency Response of an Axial-Flow Compressor Exposed to Inlet Pressure Perturbations. NASA TM X-3012, 1974.

6. Baumbick, Robert J.; Batterton, Peter G.; and Daniele, Carl J.: Terminal Shock and Restart Control of a Mach 2.5, Mixed-Compression Inlet Coupled to a Turbofan Engine. NASA TM X-3104, 1974.

7. D'Azzo, John J.; and Houpis, Constantine H.: Feedback Control System Analysis and Synthesis. Second ed. McGraw-Hill Book Co., Inc., 1966.

8. Zeller, John R.: Analysis of Dynamic Performance Limitations of Fast-Response (150 to 200 Hz) Electrohydraulic Servos. NASA TN D-5388, 1969.

9. Zeller, John R.; Webb, John A., Jr.: Determination and Evaluation of Performance Limit Criteria of Fast-Response Electrohydraulic Servosystems. NASA TM X-2736, 1973.

10. Graham, Dunstan; and McRuer, Duane: Analysis of Nonlinear Control Systems. John Wiley & Sons, Inc., 1971.

11. Thaler, George J.; and Pastel, Marvin P.: Analysis and Design of Nonlinear Feedback Control Systems. McGraw-Hill Book Co., Inc., 1962.

12. Merritt, Herbert E.: Hydraulic Control Systems. John Wiley & Sons, Inc., 1967.

13. Gebben, Vernon D.: Pressure Model of a Four-Way Spool Valve for Simulating Electrohydraulic Control Systems. NASA TN D-8306, 1976.

TABLE I. - EXAMPLE-SYSTEM PARAMETERS

| | |
|---|---|
| Example-system transfer-function coefficient, a, $\sec^2$ . . . . . . | $2.533 \times 10^{-6}$ |
| Example-system transfer-function coefficient, b, sec: | |
| At damping ratio $\zeta$ of 0.7 . . . . . . . . . . . . . . . . . . | $2.228 \times 10^{-3}$ |
| At damping ratio $\zeta$ of 0.2 . . . . . . . . . . . . . . . . . . | $6.366 \times 10^{-4}$ |
| Force level at saturation, $F_{sat}$, V . . . . . . . . . . . . . . . . . . . | 8 |
| Error gain, $K_e$ . . . . . . . . . . . . . . . . . . . . . . . . . . | 10, 5, 1 |
| Plant gain, $K_p$ . . . . . . . . . . . . . . . . . . . . . . . . . . | 50, 100, 500 |

## TABLE II. - AIRFLOW-VALVE SERVOSYSTEM PARAMETERS

Controller:
  Precompensator lead frequency, $\omega_1$, rad/sec . . . . . . . . . . . . . . . . 2π(315)
  Precompensator lead damping ratio, $\zeta$ . . . . . . . . . . . . . . . . . . . 0.50
  Precompensator lag frequency, $\omega_2$, rad/sec . . . . . . . . . . . . . . . 2π(950)
  Precompensator lag damping ratio, $\zeta$ . . . . . . . . . . . . . . . . . . . 0.50
  High-pass-filter time constant, $\tau_1$, sec . . . . . . . . . . . . . . . . . . 0.02
  Integrator low-frequency cutoff time constant, $\tau_2$, sec . . . . . . . . . . . 0.01
  Error gain, $K_e$, V/V . . . . . . . . . . . . . . . . . . . . . . . . . . . . 1.70
  Proportional to spool velocity gain, $K_{ps}$, V/V . . . . . . . . . . . . . . . 5.04
  Integral of spool velocity gain, $K_{is}$, $\text{sec}^{-1}$ . . . . . . . . . . . . . . . $1.313 \times 10^4$

Power amplifier and servovalve coil:
  Power amplifier resistors, $\Omega$
    $R_1$ . . . . . . . . . . . . . . . . . . . . . . . . . . . . . . . . . . . . 0.28
    $R_2$ . . . . . . . . . . . . . . . . . . . . . . . . . . . . . . . . . . . . 40 200
    $R_4$ . . . . . . . . . . . . . . . . . . . . . . . . . . . . . . . . . . . . 11 000
    $R_6$ . . . . . . . . . . . . . . . . . . . . . . . . . . . . . . . . . . . . 127
    $R_8$ . . . . . . . . . . . . . . . . . . . . . . . . . . . . . . . . . . . . 2000
    $R_9$ . . . . . . . . . . . . . . . . . . . . . . . . . . . . . . . . . . . . 2000
  Power amplifier voltage-to-current gain, $K_{pa}$, V/A . . . . . . . . . . . $25 \times 10^3$
  Coil resistance, $R_c$, $\Omega$ . . . . . . . . . . . . . . . . . . . . . . . . . . 3.0
  Coil inductance, $L_c$, H . . . . . . . . . . . . . . . . . . . . . . . . . . . $1.0 \times 10^{-3}$
  Coil force-to-current gain, $K_c$, N/A . . . . . . . . . . . . . . . . . . . . . 13.34

Servovalve spool dynamics:
  Spool mass, $M_s$, $\text{N} \cdot \text{sec}^2/\text{cm}$ . . . . . . . . . . . . . . . . . . . . . . $1.124 \times 10^{-3}$
  Spring rate, $K_{sp}$, N/cm . . . . . . . . . . . . . . . . . . . . . . . . . . . 4404
  Spool spring-mass system damping, $D_s$, $\text{N} \cdot \text{sec}/\text{cm}$ . . . . . . . . . . . 0.078

Servovalve orifices:
  Null flow-pressure coefficient, $K_{fp,0}$, $\text{cm}^5/\text{N} \cdot \text{sec}$ . . . . . . . . . . $7.15 \times 10^{-2}$
  Spool diameter, $d_s$, cm . . . . . . . . . . . . . . . . . . . . . . . . . . . . 1.316
  Orifice discharge coefficient, $C_d$ . . . . . . . . . . . . . . . . . . . . . . . 0.6
  Leakage orifice area at null, $\text{cm}^2$ . . . . . . . . . . . . . . . . . . . . . $1.548 \times 10^{-2}$

Hydraulic fluid:
  Hydraulic supply pressure, $P_{su}$, $\text{N}/\text{cm}^2$ . . . . . . . . . . . . . . . . . . . 2068
  Density, $\rho$, $\text{N} \cdot \text{sec}^2/\text{cm}^4$ . . . . . . . . . . . . . . . . . . . . . . . $8.175 \times 10^{-6}$
  Bulk modulus, $\beta$, $\text{N}/\text{cm}^2$ . . . . . . . . . . . . . . . . . . . . . . . $6.895 \times 10^4$

Actuator piston:
  Full stroke (zero to peak), cm . . . . . . . . . . . . . . . . . . . . . . . . . 0.318
  Area, $A_a$, $\text{cm}^2$ . . . . . . . . . . . . . . . . . . . . . . . . . . . . . . . 3.200
  Total hydraulic fluid volume in actuator, $V_t$, $\text{cm}^3$ . . . . . . . . . . . . 28.68
  Mass of piston and load-valve moving element, $M_v$, $\text{N} \cdot \text{sec}^2/\text{cm}$ . . . $1.122 \times 10^{-2}$
  Damping factor, $D_a$, $\text{N} \cdot \text{sec}/\text{cm}$ . . . . . . . . . . . . . . . . . . . . . 1.016

Transducer gains:
  Load-valve position transducer, $K_{vt}$, V/cm . . . . . . . . . . . . . . . . . 15.75
  Servovalve-spool velocity transducer, $K_{st}$, $\text{V} \cdot \text{sec}/\text{cm}$ . . . . . . . . . . 0.0472

Saturation levels:
  Coil-current saturation, $I_{c,sat}$, A . . . . . . . . . . . . . . . . . . . . . . 6.2
  Coil-voltage saturation, $E_{pa,sat}$, V . . . . . . . . . . . . . . . . . . . . . 35

TABLE III. - SUMMARY OF AIRFLOW-VALVE

LIMIT-LINE EQUATIONS

| Limit line | Equation | Value |
|---|---|---|
| Acceleration limit | $\|X_v\|\,\omega^2 = \dfrac{2\sqrt{2}\,A_a P_{su}}{3M_v}$ | $5.561 \times 10^5$ cm/sec$^2$ |
| Coil-current limit - low frequency[a] | $\|X_v\|\,\omega = \dfrac{4K_l K_c I_{c,\,sat}}{\pi K_{sp} A_a}$ | $2.407 \times 10^2$ cm/sec |
| Coil-current limit - high frequency[a] | $\|X_v\|\,\omega^3 = \dfrac{4K_l K_c I_{c,\,sat}}{\pi M_s A_a}$ | $9.430 \times 10^8$ cm/sec$^3$ |
| Coil-voltage limit - at low frequency[a] | $\|X_v\|\,\omega = \dfrac{4K_l K_c E_{pa,\,sat}}{\pi K_{sp}(R_c + R_1) A_a}$ | $4.142 \times 10^2$ cm/sec |
| Coil-voltage limit - at high frequency[a] | $\|X_v\|\,\omega^4 = \dfrac{4K_l K_c E_{pa,\,sat}}{\pi M_s L_c A_a}$ | $5.324 \times 10^{12}$ cm/sec$^4$ |

[a]Where $K_l = \pi d_s C_d \sqrt{\dfrac{2P_{su}}{3\rho}} = 3.221 \times 10^4$ cm$^2$/sec
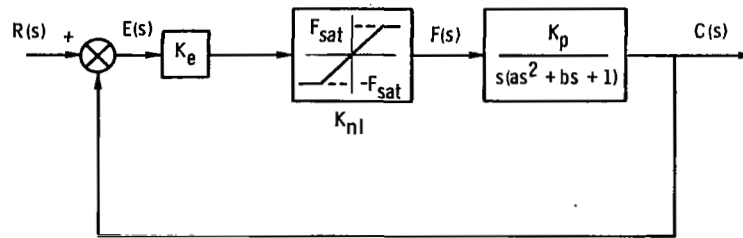
Figure 1. – Block diagram of unity-gain feedback system with saturation in forward loop.
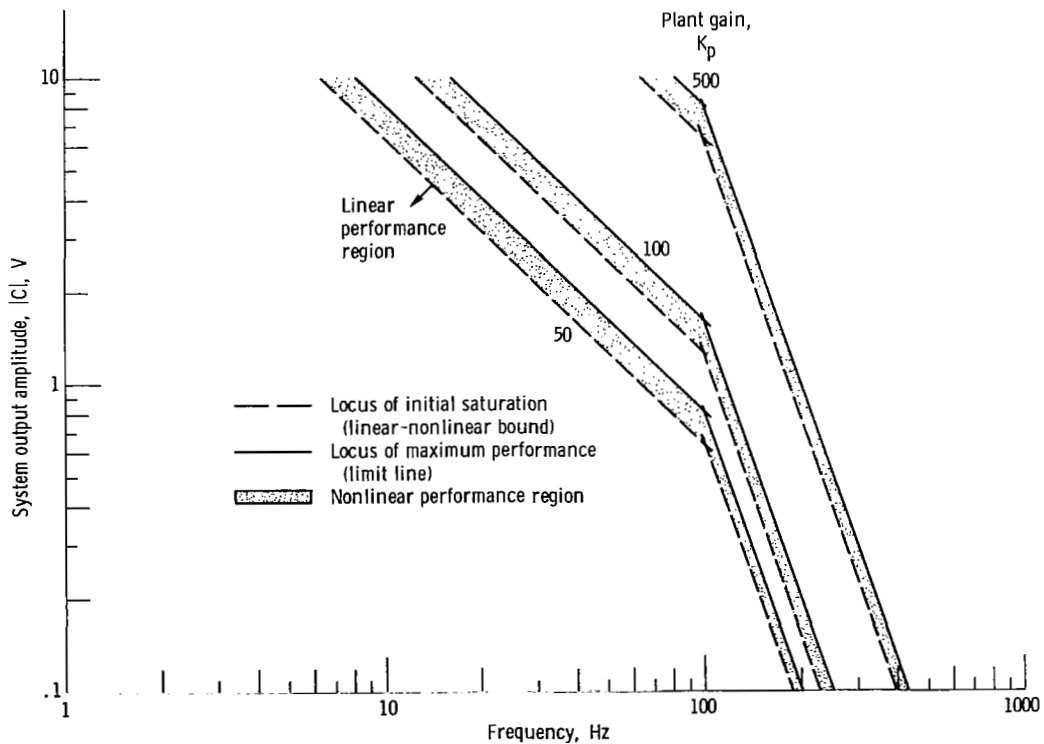


Figure 2. – Dynamic performance limit lines of example system for various plant gains.

(a) Plant gain, $K_p$, 50; error gain, $K_e$, 10.
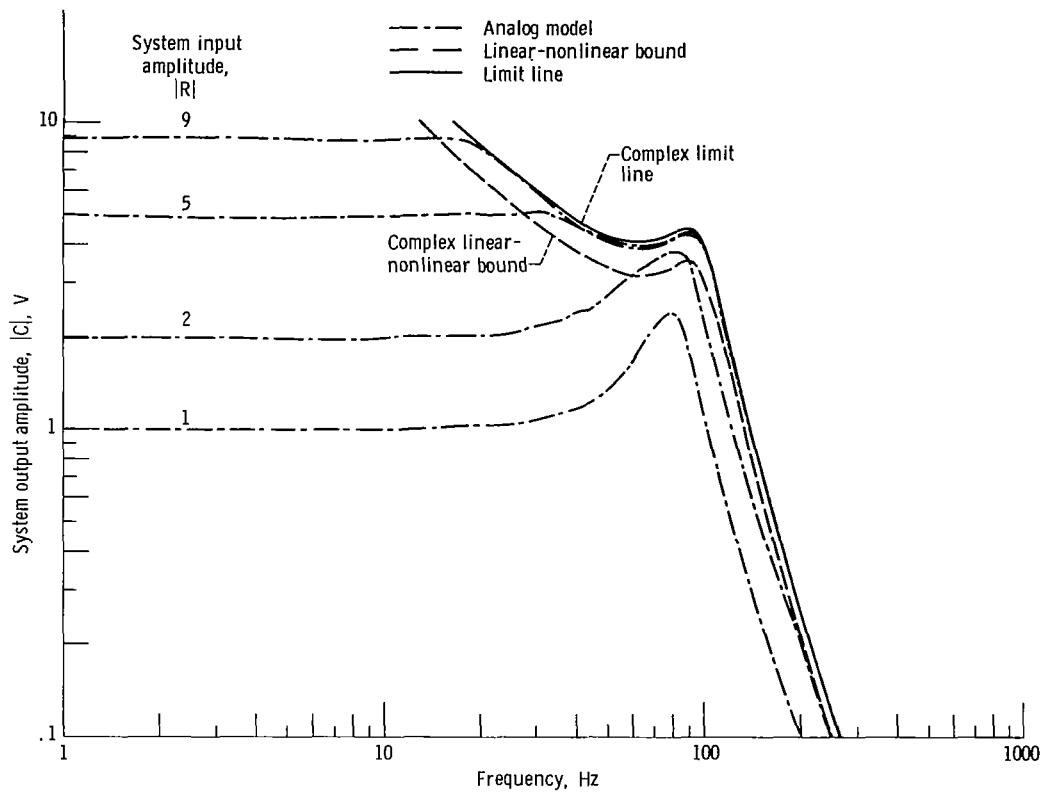
(b) Plant gain, $K_p$, 100; error gain, $K_e$, 5.
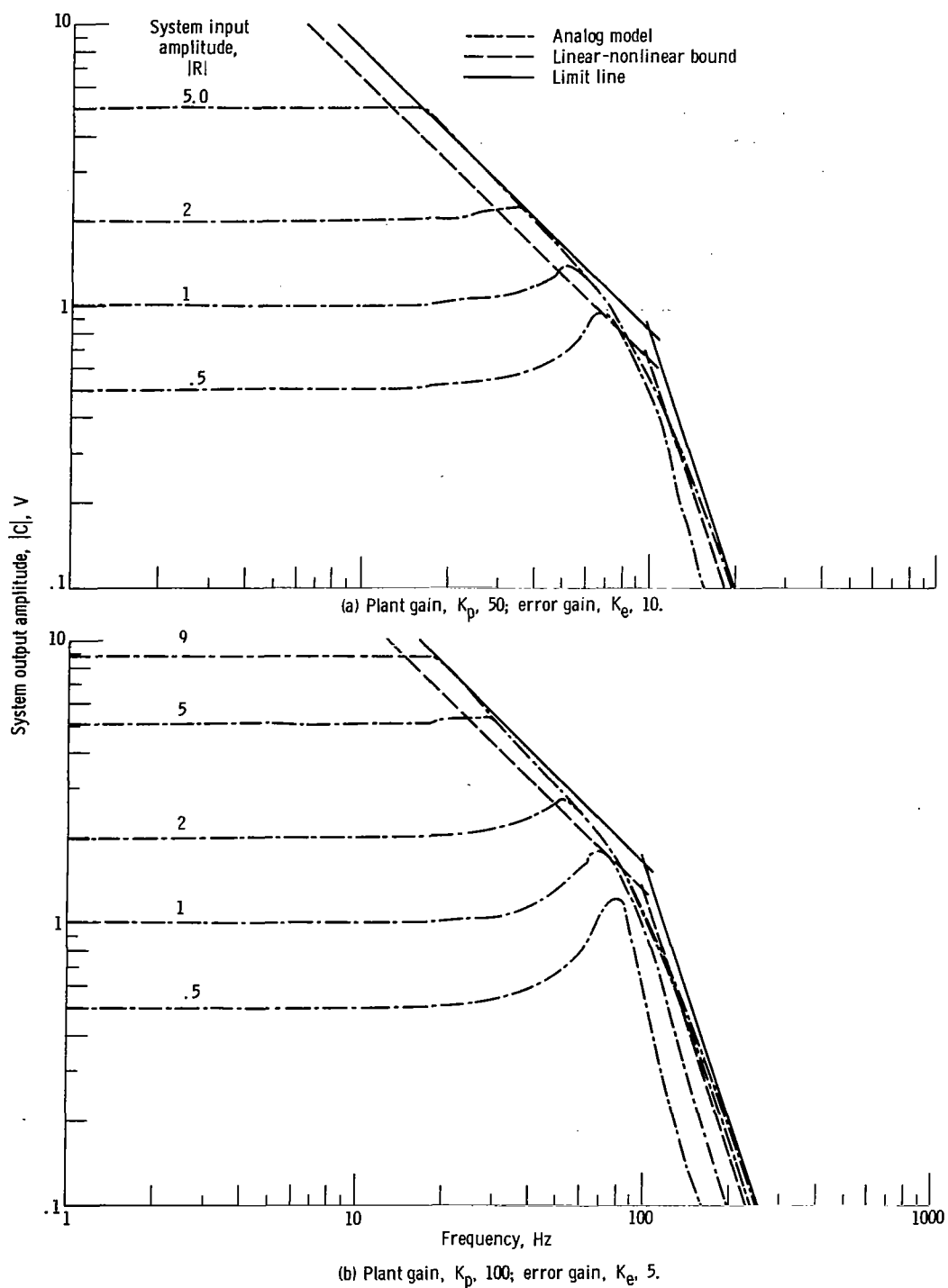
Figure 3. – Frequency response of example system from analog computer model.
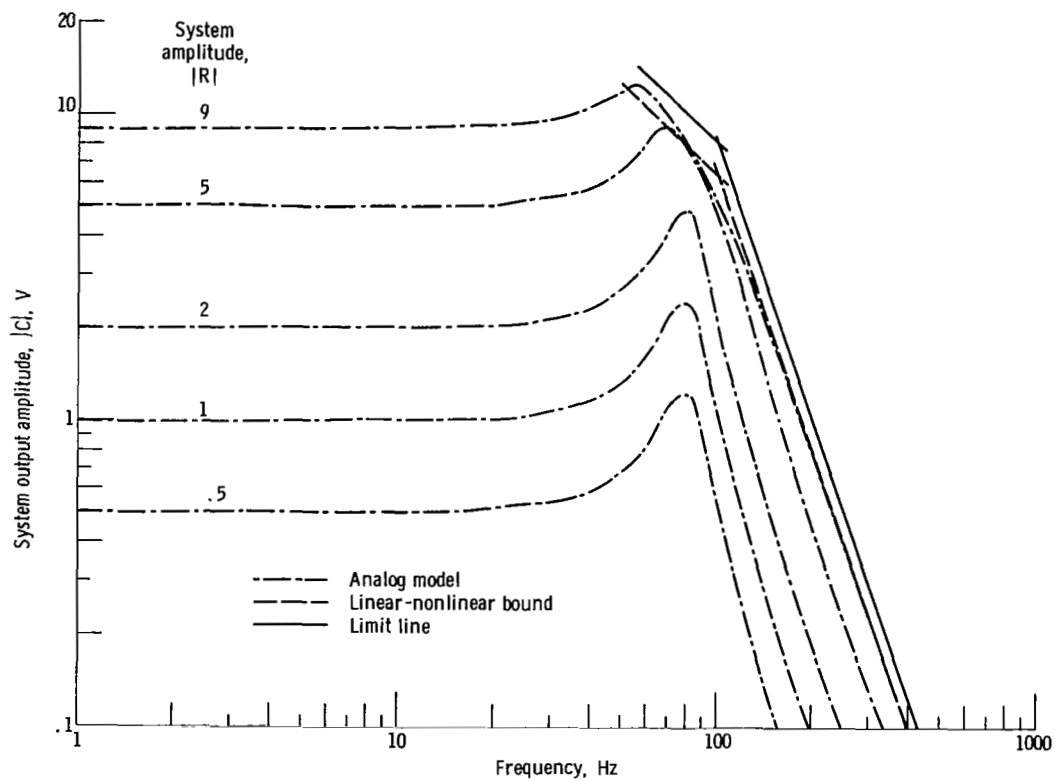
(c) Plant gain, $K_p$, 500; error gain, $K_e$, 1.

Figure 3. - Concluded.
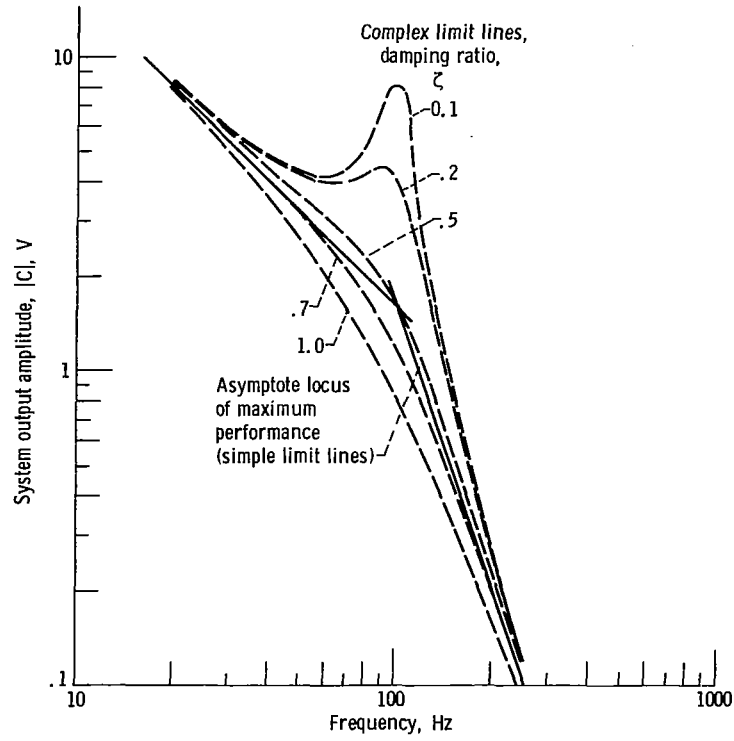
Figure 4. - Effect of plant damping on locus of maximum performance. Plant gain, $K_p$, 100; error gain, $K_e$, 5.
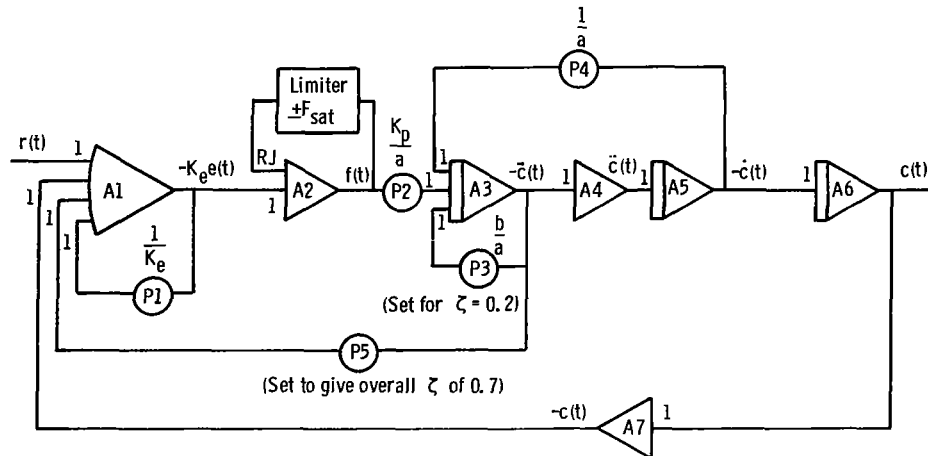


Figure 5. - Schematic of analog model for example system.

Figure 6. – Frequency response for lightly damped example system from analog computer model. Plant gain, $K_p$, 100; error gain, $K_e$, 5.

(a) Simple limit lines.  Damping ratio, $\zeta$, 0.7.

(b) Complex limit lines.  Damping ratio, $\zeta$, 0.2.
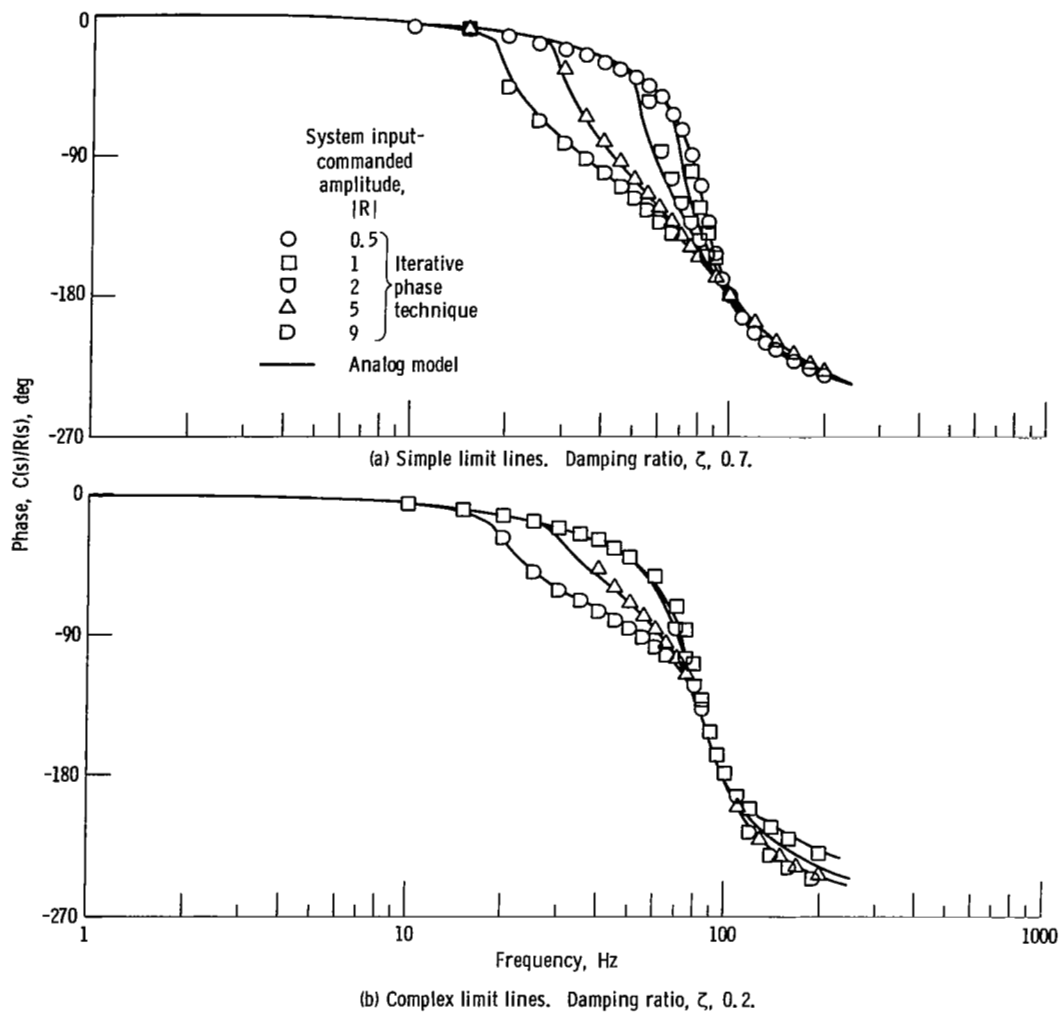
Figure 7. - Analog-computer-model phase response and approximate phase analysis.  Plant gain, $K_p$, 100; error gain, $K_e$, 5.
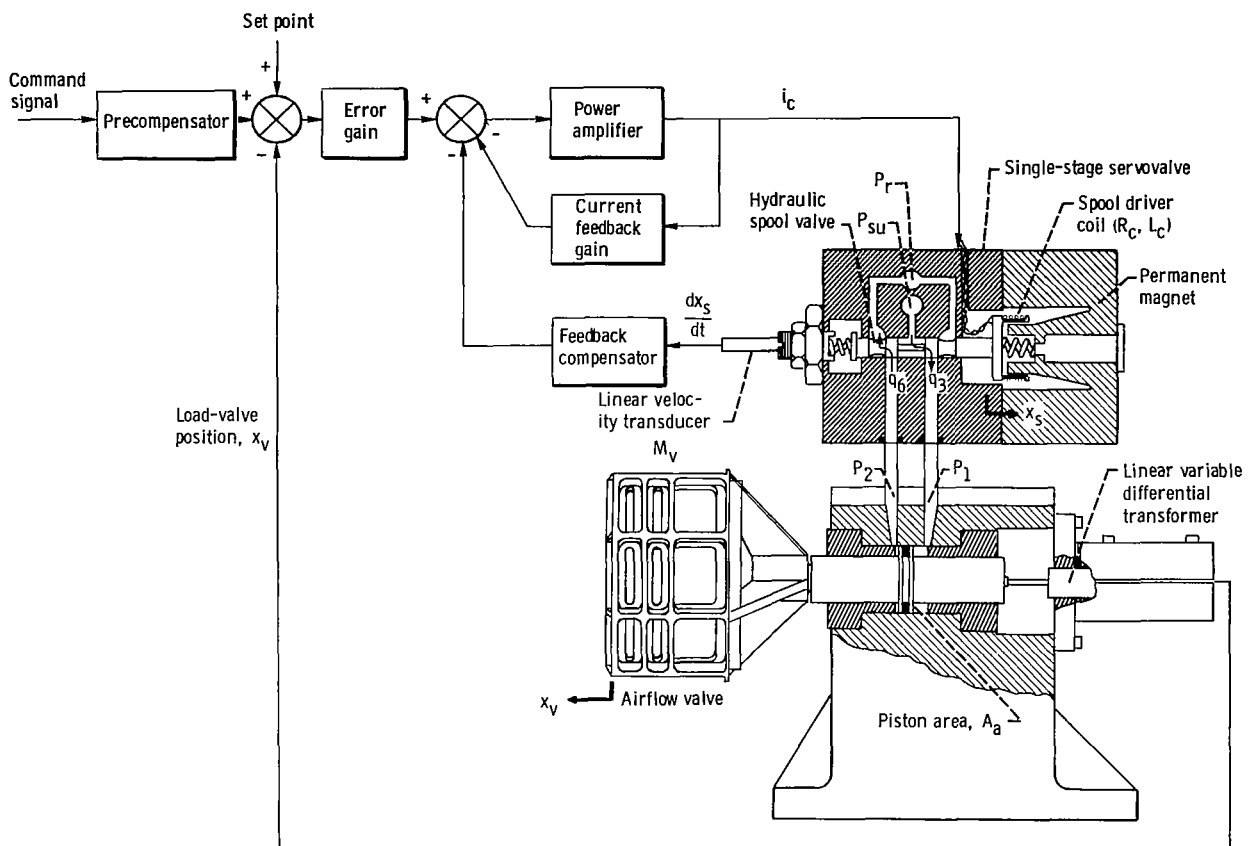
Figure 8. – Schematic diagram of electrohydraulic servosystem for positioning airflow valve.

Figure 9. – Detailed block diagram of airflow-valve servosystem.
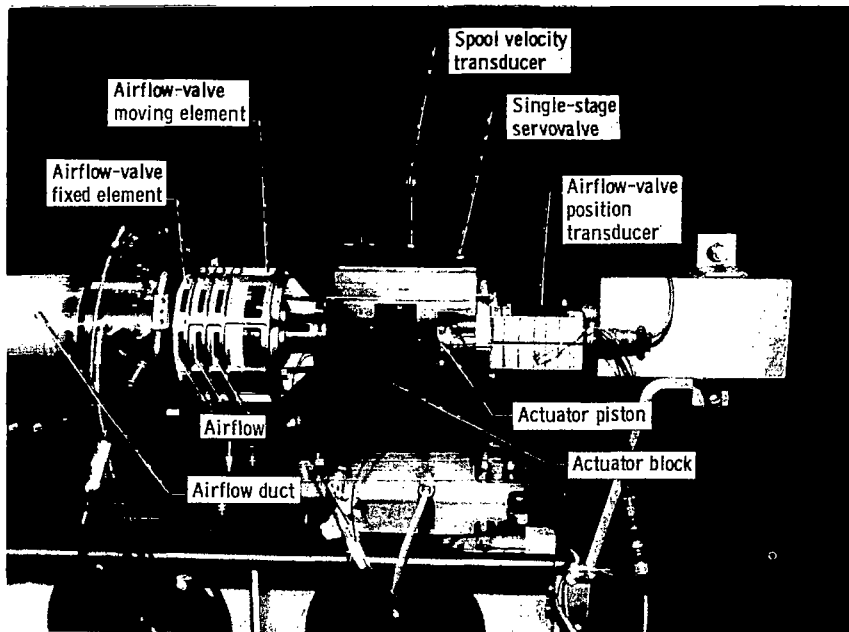
Figure 10. - Load-valve servosystem mounted on test stand.
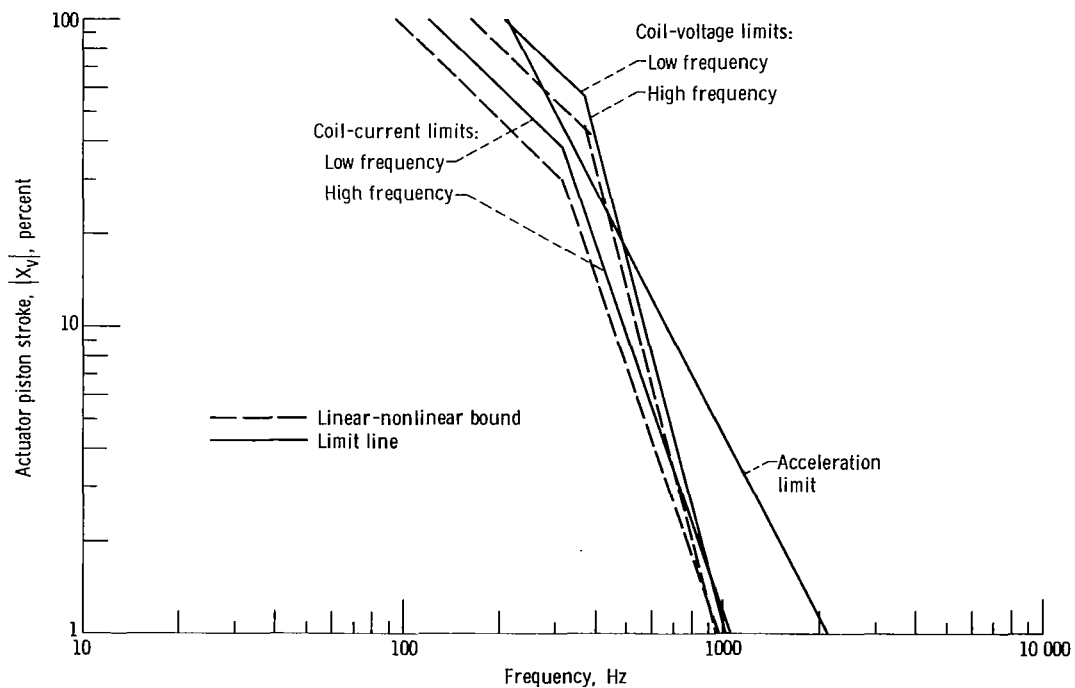


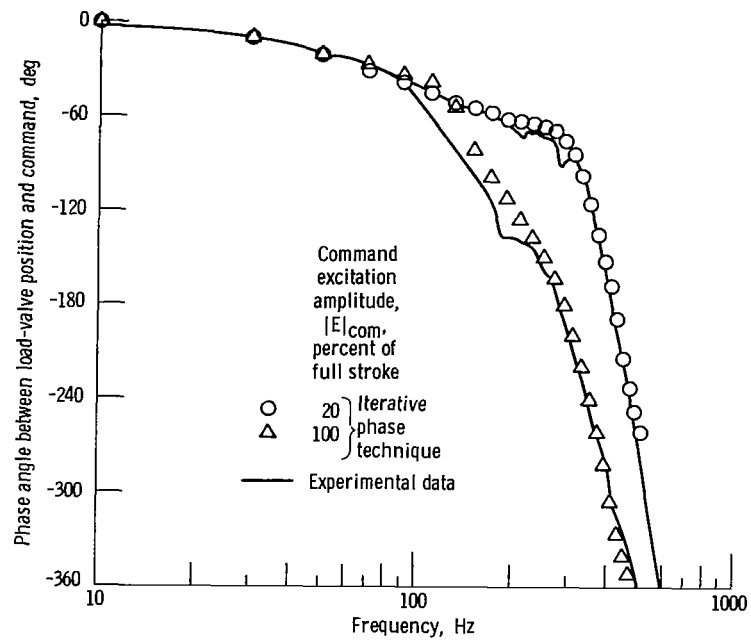Figure 11. - Limit lines for predicting dynamic performance of airflow-valve servosystem.

Figure 15. – Phase-angle response of airflow valve compared with iterative
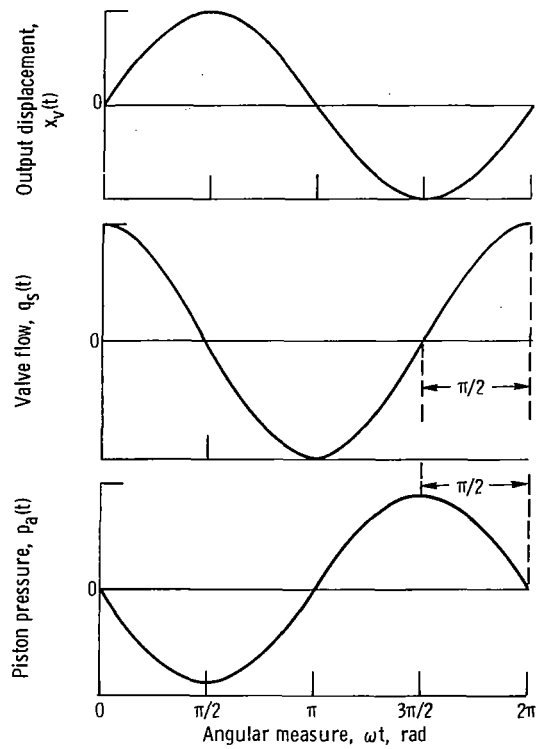analysis technique for predicting phase.



Figure 16. – Typical position, flow, and pressure
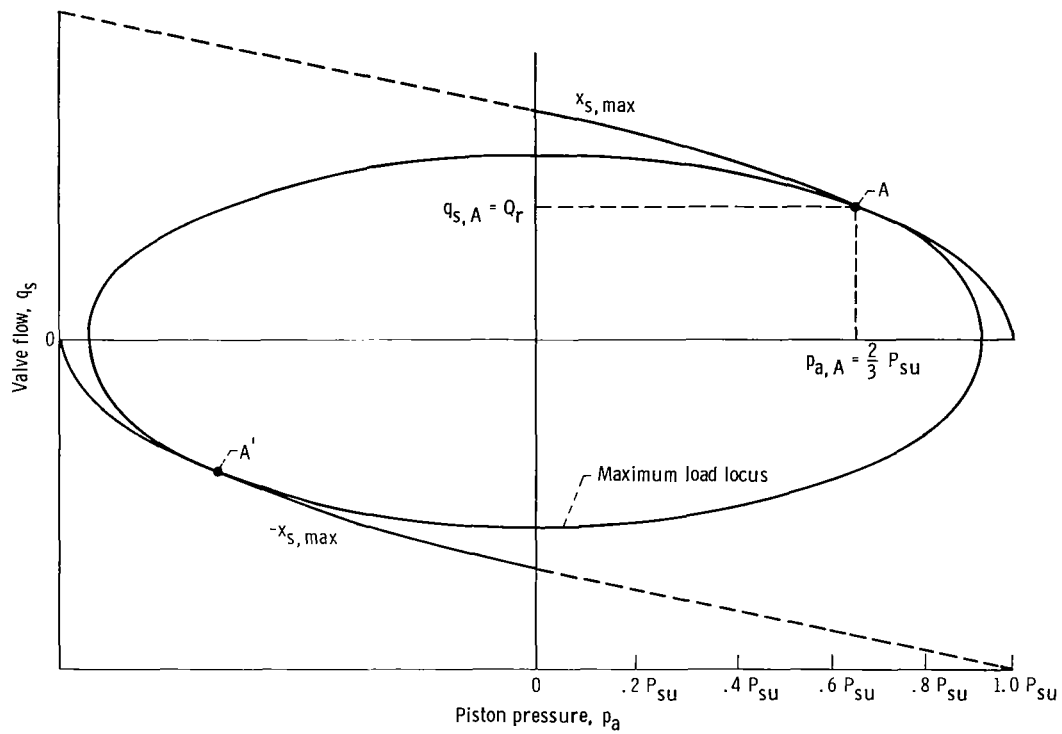response during sinusoidal motion.

Figure 17. – Servovalve maximum output capabilities and maximum load locus.

| 1. Report No. NASA TP-1488 | 2. Government Accession No. | 3. Recipient's Catalog No. |
|---|---|---|
| 4. Title and Subtitle PREDICTING DYNAMIC PERFORMANCE LIMITS FOR SERVOSYSTEMS WITH SATURATING NONLINEARITIES | | 5. Report Date July 1979 |
| | | 6. Performing Organization Code |
| 7. Author(s) John A. Webb, Jr., and Richard A. Blech | | 8. Performing Organization Report No. E-9903 |
| 9. Performing Organization Name and Address National Aeronautics and Space Administration Lewis Research Center Cleveland, Ohio 44135 | | 10. Work Unit No. 505-05 |
| | | 11. Contract or Grant No. |
| 12. Sponsoring Agency Name and Address National Aeronautics and Space Administration Washington, D.C. 20546 | | 13. Type of Report and Period Covered Technical Paper |
| | | 14. Sponsoring Agency Code |

15. Supplementary Notes

16. Abstract

This report demonstrates a technique for predicting the dynamic performance limits of a system with saturations. A generalized treatment for a system with a single saturating nonlinearity is presented and compared with frequency-response plots obtained from an analog model of the system. Once the amplitude dynamics are predicted with the limit lines, an iterative technique is employed to determine the system phase response. The saturation limit-line technique is then used in conjunction with velocity and acceleration limits to predict the performance of an electro-hydraulic servosystem containing a single-stage servovalve. Good agreement was obtained between predicted performance and experimental data.

| 17. Key Words (Suggested by Author(s)) Electrohydraulic servosystem; Servosystem; Servovalve; Fast-response system; Nonlinear; Saturation; Analysis; Control | 18. Distribution Statement Unclassified - unlimited STAR Category 08 | | |
|---|---|---|---|
| 19. Security Classif. (of this report) Unclassified | 20. Security Classif. (of this page) Unclassified | 21. No. of Pages 50 | 22. Price* A03 |

National Aeronautics and
Space Administration

Washington, D.C.
20546

Official Business
Penalty for Private Use, $300

Postage and Fees Paid
National Aeronautics and
Space Administration
NASA-451

5   1 1U,A,          072079 S00903DS
DEPT OF THE AIR FORCE
AF WEAPONS LABORATORY
ATTN: TECHNICAL LIBRARY (SUL)
KIRTLAND AFB NM 87117

# NASA